Quantum decoherence and the isotope effect in condensed phase nonadiabatic molecular dynamics simulations

Benjamin J. Schwartz,[a] Eric R. Bittner, Oleg V. Prezhdo, and Peter J. Rossky
Department of Chemistry and Biochemistry, The University of Texas at Austin, Austin, Texas 78712-1167

(Received 21 September 1995; accepted 8 January 1996)

In this paper, we explore in detail the way in which quantum decoherence is treated in different mixed quantum-classical molecular dynamics algorithms. The quantum decoherence time proves to be a key ingredient in the production of accurate nonadiabatic dynamics from computer simulations. Based on a short time expansion to a semiclassical golden rule expression due to Neria and Nitzan [J. Chem. Phys. **99**, 1109 (1993)], we develop a new computationally efficient method for estimating the decay of quantum coherence in condensed phase molecular simulations. Using the hydrated electron as an example, application of this method finds that quantum decoherence times are on the order of a few femtoseconds for condensed phase chemical systems and that they play a direct role in determining nonadiabatic transition rates. The decay of quantum coherence for the solvated electron is found to take $\approx$50% longer in D_2O than in H_2O, providing a rationalization for a long standing puzzle concerning the lack of experimentally observed isotope effect on the nonadiabatic transition rate: Although the nonadiabatic coupling is smaller in D_2O due to smaller nuclear velocities, the smaller coupling in D_2O adds coherently for a longer time than in H_2O, leading to nearly identical nonadiabatic transition rates. The implications of this isotope dependence of the nonadiabatic transition rate on changes in the quantum decoherence time for electron transfer and other important chemical reactions are discussed. [S0021-9606(96)51514-5]

I. INTRODUCTION

In many condensed phase chemical systems, it is possible to simulate the physics and chemistry of interest by treating a few select degrees of freedom quantum mechanically while treating the remainder classically.[1] This is desirable since it is not yet computationally practical to treat a condensed system entirely quantum mechanically, and a purely classical treatment misses much of the relevant physical phenomena. In such a mixed quantum-classical simulation, the positions of the classical degrees of freedom define a potential energy surface for the quantum subsystem of interest, while changes of the quantum subsystem in turn affect the classical dynamics. Whenever the energy of the classical motions coupled to the quantum system is comparable to the quantum energy gap, energy transfer can take place between the quantum and classical degrees of freedom.[2] This type of radiationless or nonadiabatic transition of the quantum subsystem, corresponding to a breakdown of the Born–Oppenheimer approximation for a quantum subsystem, plays an important role in many fundamental chemical processes including internal conversion, electron, proton, and other charge transfer reactions, electronic energy transfer, and intramolecular energy redistribution.

One of the key issues in describing nonadiabatic transitions in the condensed phase is the proper treatment of the short-lived phase coherence between the quantum wave function and the classical (bath) degrees of freedom.[3] In the following discussion, we will assume without loss of generality that we are considering a quantum electronic system and a classical nuclear bath. In such mixed quantum-classical systems, the nuclear dynamics follows according to a given adiabatic potential surface associated with one of the eigenstates of the electronic Hamiltonian. Thus the potential felt by the nuclear degrees of freedom will depend strongly upon the quantum state of the electronic degrees of freedom. The fundamental distinction between quantum mechanics and classical mechanics is that a quantum system can evolve into a coherent linear superposition of states. Quantum mechanically, the effects of all alternative histories associated with this coherent superposition, including those of the (classical) bath, must be considered. As the electronic wave function evolves from an initially pure eigenstate to a coherent superposition of eigenstates, alternative paths for the nuclei emerge: Each path is associated with dynamics arising from starting in an initial nuclear configuration and electronic state and ending in a different final nuclear configuration and final electronic state. The nuclear dynamics for the different quantum paths diverge in both position and phase, leading to destructive interference between the nuclear wave functions associated with these paths. This effect is known as quantum decoherence.[4]

Since quantum decoherence acts to dissipate long lived superpositions of states, it profoundly diminishes the transition probability between quantum states which are coupled by the nuclear dynamics.[3,5] Correspondingly, when the loss of quantum phase coherence between the electronic and nuclear degrees of freedom is neglected, which is a typical approximation made in many mixed quantum-classical treatments,[6] the expected result will be an incorrect estimate

[a]Present address: Institute for Polymers and Organic Solids, University of California at Santa Barbara, Santa Barbara, CA 93106-5090.

 0021-9606/96/104(15)/5942/14/$10.00

of the transition probabilities and other associated physical observables. Because of the tremendous utility of mixed quantum-classical treatments in simulating condensed phase phenomena, it is thus of paramount importance to be able to properly incorporate the effects of quantum decoherence in such simulations.

The purpose of this paper is to explore the approximations inherent in the treatment of quantum decoherence in mixed quantum-classical computer simulations to better understand the role of decoherence in fundamental nonadiabatic chemical processes. In the following section, several methods for estimating nonadiabatic transition rates using molecular dynamics are discussed, and the assumptions in each for dealing with the issue of quantum decoherence are made explicit. Central to all the methods is the issue of the decoherence time scale: that is, over which time scale must one consider the quantum phase evolution of the bath in computing transition probabilities? Section III presents a new, computationally efficient method for estimating the decoherence time based on extension of a golden rule formalism originally developed by Neria and Nitzan.[7–9] This new method is illustrated in Sec. IV utilizing the paradigm of nonadiabatic condensed phase systems, the hydrated electron. Section V demonstrates the role of the isotope effect in altering both the decoherence time and the magnitude of the nonadiabatic coupling in the hydrated electron system, a result which provides an explanation for the observed lack of an isotope effect on the nonadiabatic transition rate in recent femtosecond experiments. Finally, Sec. VI discusses the potentially profound implications of this effect for many chemical systems, especially electron transfer reactions, and summarizes the importance of correctly treating quantum decoherence in nonadiabatic computer simulations.

II. MOLECULAR DYNAMICS AND NONADIABATIC TRANSITIONS

Due to the fundamental role of radiationless processes in chemical reactivity, there is a large literature devoted to extracting nonadiabatic dynamical information from computer simulations.[2,5–15] The approaches considered in this section fall into two general categories: nonadiabatic rate estimates based on perturbation theory,[7–10] and dynamical algorithms which incorporate electronic transitions.[5,6,11–15]

The first methods summarized utilize perturbation theory to provide an expression for the radiationless transition rate in terms of nonadiabatic coupling matrix elements, which are in turn evaluated by computer simulations on individual adiabatic surfaces.[7–10] Although this class of methods do not provide nonadiabatic molecular dynamics *per se*, they offer utility in a semiclassical determination of electronic transition rates, especially for systems where the magnitude of the nonadiabatic coupling is small. Many of the concepts underlying quantum decoherence as well as the basis for our new method for estimating decoherence times are readily illustrated in the perturbative golden rule formalism, so we devote particular attention to it below.

The second class of methods provide access to dynamical quantities by providing an algorithm for mixed quantum-classical molecular simulations with the inclusion of nonadiabatic transitions.[5,6,11–15] Due to the divergence of classical trajectories propagated under the influence of different electronic states of the quantum system, running classical trajectories on a single weighted adiabatic potential is usually inadequate to describe the physics of interest.[12] To account for this, the techniques discussed below incorporate stochastic surface hopping, where the probability of dynamically hopping to a different electronic surface depends on nonadiabatic coupling coefficients computed during the course of the trajectory. Both the classical dynamics and the nonadiabatic transition probabilities depend directly on how these algorithms treat quantum coherence. Thus the decoherence time plays a direct role in determining physical properties calculated from ensemble averages of nonadiabatic computer trajectories.

A. Semiclassical transition rates from Fermi's golden rule

For a generalized mixed quantum-classical system, the quantum mechanical coordinates of interest will be specified by **r**, while the remaining classical degrees of freedom will be labeled **R**. The language we use throughout this paper refers to the quantum coordinates as ''electronic'' (although any quantized coordinate, such as a high frequency vibration, could also be used) and the classical coordinates as the nuclear, or ''bath.'' The Hamiltonian for this mixed system is given by

$$H = H_0(\mathbf{r};\mathbf{R}) + T(\mathbf{R}), \tag{1}$$

where $H_0(\mathbf{r};\mathbf{R})$ is the electronic Hamiltonian for a given set of nuclear positions **R**, and $T(\mathbf{R})$ is the nuclear kinetic energy operator. In the adiabatic approximation, the coupling of different electronic states through the nuclear kinetic energy operator, $T(\mathbf{R})$, is neglected. Under this approximation, the adiabatic states are defined as $|\alpha_i\rangle$

$$H_0(\mathbf{r};\mathbf{R})|\alpha_i\rangle = E_i|\alpha_i\rangle, \tag{2}$$

where i labels a particular electronic state and the explicit dependence on the electronic coordinate, **r**, has been dropped for notational convenience. Within the adiabatic basis, $\{\alpha_i(\mathbf{R})\}$, the nonadiabatic coupling matrix elements T_{ij} are defined as

$$\begin{aligned} T_{ij} &= \langle \alpha_i(\mathbf{R})|T(\mathbf{R})|\alpha_j(\mathbf{R})\rangle \\ &= -\sum_n \frac{\hbar^2}{2M_n}\langle \alpha_i(\mathbf{R})|\frac{\partial^2}{\partial \mathbf{R}^2}|\alpha_j(\mathbf{R})\rangle, \end{aligned} \tag{3}$$

where the T_{ij} are operators on the nuclear subspace and the sum runs over all the nuclei which have masses M_n.

Using first order time dependent perturbation theory,[16] the nonadiabatic transition rate, k_{ij}, between an initial electronic surface $|\alpha_i\rangle$ and another electronic surface $|\alpha_j\rangle$ can be described by the golden rule

$$k_{ij}=\frac{2\pi}{\hbar}\sum_{F}\langle\alpha_i(\mathbf{R})I(\mathbf{R})|T(\mathbf{R})|\alpha_j(\mathbf{R})F(\mathbf{R})\rangle|^2\delta(E_i-E_f), \tag{4}$$

where $|I(\mathbf{R})\rangle$ and $|F(\mathbf{R})\rangle$ are the nuclear states associated with the initial and final electronic states which have energies E_i and E_j, respectively. [Note that a thermal rate constant would also involve a Boltzmann average over the initial electronic state which has not been included in Eq. (4).] By using the Fourier representation of the delta function and the first equality of Eq. (3) in Eq. (4), and then performing the sum over final states, the golden rule expression becomes

$$k_{ij}=\int_{-\infty}^{\infty}dt\langle I(\mathbf{R})|T_{ij}(\mathbf{R})e^{iH_jt/\hbar}T_{ji}(\mathbf{R})e^{-iH_it/\hbar}|I(\mathbf{R})\rangle, \tag{5}$$

where H_i and H_j are the nuclear Hamiltonians associated with the two electronic states and are assumed to be defined from a common energy origin. We note that the nuclear coordinates $\mathbf{R}=\mathbf{R}(t)$ are parametrized by time. Equation (5), which is the starting point for many nonadiabatic calculations in the literature,[1,7,8,10] can be converted into a more useful form for our purposes by using the second equality of Eq. (3), employing the chain rule for differentiation and neglecting the higher order terms involving second derivatives[7,8]

$$k_{ij}=\int_{-\infty}^{\infty}dt\Big\langle\sum_n\sum_m \boldsymbol{F}_n(\mathbf{R}^{(j)}(t))\cdot\mathbf{v}_n^{(j)}(t) \times\boldsymbol{F}_m(\mathbf{R}^{(i)}(0))\cdot\mathbf{v}_m^{(i)}(0)J(t)\Big\rangle, \tag{6}$$

where

$$\boldsymbol{F}_n(\mathbf{R}^{(i)}(t))=i\langle\alpha_i|\frac{\partial H_0}{\partial\mathbf{R}_n^{(i)}}|\alpha_j\rangle. \tag{7}$$

In the above expression, the angled brackets indicate an ensemble average over initial conditions, the sums run over the different nuclei, $\mathbf{v}_n^{(i)}(t)$ is the velocity of nucleus n evaluated after propagation along electronic surface i for time t, $F_n(\mathbf{R}^{(i)}(t))$ is the matrix element of the ''force'' on nucleus n (which has been propagated for time t along surface i) evaluated between the two adiabatic states, and

$$J(t)=\langle I(\mathbf{R}(0))|e^{iH_jt/\hbar}e^{-iH_it/\hbar}|I(\mathbf{R}(0))\rangle. \tag{8}$$

Equation (8) for $J(t)$, the time-dependent overlap of the nuclear wave function propagated on the two different surfaces, makes use of the fact that the nuclear positions on both states i and j are identical at time zero.

The physical interpretation underlying Eq. (6) is relatively straightforward. The system is initially in electronic state i at time zero, and the classical coordinates have positions $\mathbf{R}^{(i)}(0)$ and velocities $\mathbf{v}^{(i)}(0)$. The nonadiabatic coupling is given by a complex number, $\mathbf{F}\cdot\mathbf{v}$, which is proportional to the projection of the nuclear velocities along the force matrix element between the two states. In general, the two surfaces are more strongly mixed when $\mathbf{F}$ is large, leading to a larger integrand for the transition rate between the adiabatic states. Increasing the nuclear velocities also increases the integrand, as expected (the rate should be higher in the presence of faster nuclear motions due to breakdown of the adiabatic approximation), but only the component of the velocity along the nonadiabatic force matrix element contributes. The overall rate is proportional to the time integral of the autocorrelation of the coupling: The rate depends on the decay of the correlation of $\mathbf{F}\cdot\mathbf{v}$ evaluated at time zero on surface i and $\mathbf{F}\cdot\mathbf{v}$ evaluated at time t on surface j. Thus not only is the magnitude of the coupling term important to the rate, but so is the time over which the two surfaces remain strongly coupled. Propagation on the two different electronic surfaces will lead to divergent nuclear velocities and nonadiabatic force matrix elements, so the $\mathbf{F}\cdot\mathbf{v}$ coupling terms evaluated on the two surfaces eventually become uncorrelated. It is also important to note that there generally is interference between successive regions of nonadiabatic coupling: Contributions to the integrand at later times could add either constructively or destructively to those from earlier times, potentially producing a large effect on the overall transition rate.

Inspection of Eq. (6) also reveals that the overall nonadiabatic transition rate is also modulated by the $J(t)$ term. Starting with a given set of nuclear positions $\mathbf{R}$ at time zero and noting that by definition $J(0)=1$, it is evident that $J(t)$ provides a measure of how the overlap of the nuclear wave functions on the two surfaces decays as the nuclear positions and phases diverge due to propagation with the two different electronic Hamiltonians. Of particular importance, because $J(t)$ enters multiplicatively into the integrand in Eq. (6), the decay of $J(t)$ presents an upper limit for the time over which coupling between the surfaces affects the transition rate. We will show below that, for the example of the hydrated electron, $J(t)$ does indeed decay on a time scale faster than the autocorrelation of the nonadiabatic coupling matrix elements and hence plays an important role in determining the nonadiabatic transition rate. We define the time scale set by the decay of $J(t)$ as the quantum decoherence time. In most nonadiabatic molecular dynamics simulations, however, there are no nuclear wave functions with which to evaluate this decoherence term. Thus mixed quantum-classical computer simulations have relied on assumptions to incorporate the effects of decoherence into nonadiabatic dynamics and the estimation of radiationless transition rates.[2,6,12–15]

B. Nonadiabatic molecular dynamics simulations

In a mixed quantum-classical simulation, the positions of the classical nuclei define an instantaneous classical potential energy surface for the quantum degrees of freedom. As the bath particles move, the energies associated with the instantaneous adiabatic electronic eigenstates will change. If the quantum system is prepared in an adiabatic eigenstate, the coupling between the electronic states due to nuclear motion of the bath particles generally produces a mixed quantum state in the adiabatic basis at later times. Because the classical particles are constrained to evolve only on the individual adiabatic potential energy surfaces, a mixed quantum super-

position provides many alternative instantaneous classical pathways or histories. The divergence of these alternative classical histories and the associated loss of phase coherence between them causes quantum decoherence.[5] By decoherence we mean there is a dissipation of contributions due to quantum mechanical phase interference between the alternative histories. Sets of histories which have lost coherence are termed ''coarse grained'' and their associated weights are summed together as ordinary probabilities as opposed to quantum mechanical amplitudes.[17] The effect of this coarse graining is the projection of the quantum system into an adiabatic eigenstate (since outside of regions of strong coupling, the system must eventually be described by probabilities for occupation of alternative electronic eigenstates). Thus, the coupling to the bath serves both to destroy adiabaticity by producing quantum superposition states from an initial adiabatic eigenstate, and to restore adiabaticity by eliminating the coherences in the superposition via coarse graining, which resolves the quantum system back into instantaneous adiabatic eigenstates.[5,17] If the mixed quantum state is comprised of a fraction of the initial adiabatic state with components of other adiabatic states, there will be some probability that the collapsed wave function corresponds to a different final adiabatic state. This view of mixed quantum-classical dynamics, where adiabatic states evolve into quantum mixed states and are subsequently projected back into a new adiabatic basis, forms the essence underlying surface hopping molecular dynamics algorithms. The important role of quantum coherence can be demonstrated in two such algorithms: the ''fewest switches'' or MDET (molecular dynamics with electronic transitions) algorithm,[5,6,12] and the stationary phase surface hopping approach.[13–15]

In the fewest switches algorithm, pioneered by Tully[12] and further developed by Coker and co-workers,[6] complex coefficients are used to describe the (generally) mixed state quantum system for a given position of the classical coordinates. Thus, the mixed quantum state at a given time can be described in terms of the adiabatic basis,

$$|\psi_i(t)\rangle = \sum_i c_i(t)|\alpha_i\rangle. \tag{9}$$

Representing the complex coefficients in density matrix notation, $\rho_{ij}=c_i c_{ij}^*$ and substituting Eq. (9) into the time-dependent Schrödinger equation provides equations of motion for coherent propagation of the complex coefficients under the influence of the bath

$$\frac{\partial}{\partial t}\rho_{ij} = \sum_k (\rho_{ij}\mathbf{R}\cdot\mathbf{d}_{ik} - \rho_{ik}\mathbf{R}\cdot\mathbf{d}_{kj}) - i(E_i - E_j)\rho_{ij}, \tag{10}$$

where the nonadiabatic coupling vector between states i and k is given by

$$\mathbf{d}_{ik} = \langle \alpha_i|\boldsymbol{\nabla}_R|\alpha_k\rangle, \tag{11}$$

where the gradient is taken with respect to the classical coordinates. Propagation of the classical particles is performed adiabatically using the Hellmann–Feynman force

$$\boldsymbol{F}_Q^{(i)}(\mathbf{R}) = -\langle \alpha_i|\boldsymbol{\nabla}_R H|\alpha_i\rangle, \tag{12}$$

where $\boldsymbol{F}_{\mathrm{Q}}^{(\mathrm{i})}(\mathbf{R})$ is the force on the classical coordinates $\mathbf{R}$ due to the quantum system in adiabatic state i, and the system Hamiltonian $H=H(\mathbf{r};\mathbf{R})$ is as defined in Eq. (1). The algorithm then incorporates surface hopping, where the probabilities to hop between adiabatic surfaces, g_{ij}, are chosen to produce the correct distribution of ensemble members consistent with the coherently propagated mixed wave function,

$$g_{ij} = \frac{2}{\hbar}\frac{\Delta t}{\rho_{ii}}\mathrm{Re}[\rho_{ji}^*\mathbf{R}\cdot\mathbf{d}_{ij}]\Theta(-\mathrm{Re}[\rho_{ji}^*\mathbf{R}\cdot\mathbf{d}_{ij})]), \tag{13}$$

where Δt is the time step, and $\Theta(x)$ is the Heaviside step function which ensures the system undergoes the fewest number of transitions between adiabatic states.

To produce nonadiabatic dynamics with the fewest switches algorithm, the system generally begins in an adiabatic eigenstate, and then the classical nuclear and quantum dynamics are propagated for one time step using Eq. (12) and Eq. (10).[12] This produces a mixed quantum state at the end of the step, so surface hopping is used to select an adiabatic state for propagating the next step by comparing the quantity g_{ij} from Eq. (13) to a random number. If no switch between states is made, propagation simply continues to the next step. If a switch between states i and j occurs, the energy excess or deficit in the quantum coordinates is distributed among the classical coordinates along the nonadiabatic coupling vector $\mathbf{d}_{ij}$, defined in Eq. (11),[18,19] and then propagation continues using the new quantum state. The values of the complex coefficients, ρ_{ij}, are retained throughout the propagation, so that memory of the coupling between states at different times is preserved: The entire trajectory is propagated completely coherently. To account for decoherence then, it would be necessary to evaluate an entire swarm of trajectories from the same (classical) initial condition. Different random number sequences would produce different transition points in the different trajectories of the swarm. Since the classical dynamics between trajectories with transitions in different places will generally diverge, the interference between all the trajectories in the swarm, when summed together, would provide a natural description of quantum decoherence for the initial time step.[6,12]

This natural description of quantum decoherence, however, comes at a computational price. To obtain ensemble properties of a mixed quantum-classical system, a thermal distribution of initial configurations must be chosen, and then a swarm of trajectories run for each initial condition. The properties of the system as a whole consist of ensemble averages of the sums of the swarm of trajectories associated with each initial condition. Especially for cases where the coupling is weak or the decoherence time is short, one expects that a very large swarm of trajectories would be required from each initial condition to correctly damp out memory of the nonadiabatic transition amplitudes between different times. Moreover, it is not clear *a priori* how many trajectories would be required for a given initial condition to ensure that coherence has been properly damped. A new nonadiabatic method recently developed by two of us recasts the fewest switches algorithm in a formalism where a single

trajectory can be propagated with smooth damping of quantum coherence as long as the decoherence time is known in advance.[5]

In the stationary phase surface hopping approach, pioneered by Webster *et al.*[13,14] and generalized recently to include approximate eigenstates by Murphrey and Rossky,[15] the classical dynamics are propagated under the influence of the mixed quantum state rather than adiabatically. The algorithm utilizes an expression for the quantum force developed by Pechukas[20] using the stationary phase approximation in a path integral representation of the quantum propagator $U(t,t_0)$,

$$\mathbf{F}_Q(t') = \frac{-\mathrm{Re}[\langle \alpha_j(\mathbf{R}(t))|U(t,t')\nabla_R H_0[\mathbf{R}(t)]U(t',t_0)|\alpha_i(\mathbf{R}(t_0))\rangle]}{\langle \alpha_j(\mathbf{R}(t))|U(t,t_0)|\alpha_i(R(t_0))\rangle}. \tag{14}$$

This expression for the force is then combined with the surface hopping algorithm of Tully and Preston,[11] where the hopping probabilities are computed from the magnitudes of the overlap of the initial adiabatic state projected onto the possible final adiabatic states

$$T_{ij} = \langle \alpha_j(\mathbf{R}(t))|U(t,t_0)|\alpha_i(\mathbf{R},t_0))\rangle. \tag{15}$$

The Pechukas force expression, Eq. (14), also conserves energy and angular momentum during an electronic transition ($i \neq j$); the force on the classical particles reflects the smooth evolution of the initial adiabatic state into a quantum mixed state which is eventually resolved into a new adiabatic state at the end of the time step.

To produce nonadiabatic dynamics with the stationary phase surface hopping algorithm, it must be noted that Eq. (14) is nonlocal in time: The force acting on the classical nuclei over the step time $\Delta t = t - t_o$ depends on the adiabatic wave functions (which in turn depend on the nuclear coordinates) at both the initial time t_o and the final time t. The system generally begins in an adiabatic eigenstate, and the classical dynamics are propagated under a linearized Hamiltonian to determine the approximate final adiabatic eigenstates. The final adiabatic state j is chosen by computing T_{ij} from Eq. (15) and comparing to a random number. The value of j thus determined is then used in Eq. (14), which is solved self-consistently for the classical and quantum dynamics. This algorithm provides for complete quantum coherence during the time step, with the selection of the final adiabatic eigenstate at the end of each step. The transition probabilities computed over a given time step with the stationary phase surface hopping method are equivalent to those produced by the swarm of trajectories necessary in the fewest switches approach. Like the fewest switches algorithm, the complex amplitudes for the transition probabilities from Eq. (15) could then be retained and added over an arbitrary number of subsequent time steps, preserving coherence. The typical use of the stationary phase surface hopping algorithm, however, includes dropping the complex phases at the end of each time step to provide for natural decoherence with a single nonadiabatic trajectory.[13–15]

The chief concern when employing the stationary phase surface hopping algorithm lies in the choice of the quantum decoherence time. As will be demonstrated in the next section, complex interferences between the transition amplitudes along consecutive time steps can lead to an overall electronic transition probability which depends directly on the coherence time. Thus nonadiabatic transition rates and dynamical quantities computed with this algorithm will in general be a function of the chosen decoherence time. Clearly, for both the stationary phase surface hopping and fewest switches algorithms, an independent method for estimating the quantum decoherence time is required. We propose such a method in the following section.

III. ESTIMATING QUANTUM DECOHERENCE TIMES

In order to estimate the quantum decoherence time for either the stationary phase surface hopping or fewest switches molecular dynamics simulations, it is necessary to make some type of semiclassical approximation for the nuclear degrees of freedom. The approach we will take, following that of Neria and Nitzan,[7–9] relies on a semiclassical approximation for calculating the nuclear wave function of the bath. Since the bath wave function enters directly into the golden rule expression for the nonadiabatic transition rate, Eq. (6), the quantum coherence time can be determined simply from the decay of the nuclear function $J(t)$.

At the heart of the method is the estimation of the nuclear wave function of the solvent based on Heller's frozen Gaussian approximation (FGA).[21] Heller showed that Gaussian wave packets, centered on the positions of simulated classical particles and propagated classically, can be used successfully to calculate many quantum properties of complex systems. This approximation works well for short times when there is negligible spreading of the nuclear wave packets. Since decoherence times in condensed phase systems are on the order of a few femtoseconds (as will be demonstrated for the case of the hydrated electron in the next section), we expect this will be an excellent approximation. The nuclear wave function of the bath, then, is given by the superposition of the frozen Gaussians, $G_n^{(i)}(\mathbf{x},\mathbf{p};t)$, centered on the individual nuclei and propagated on electronic surface i,[7–9]

$$\langle \mathbf{R}|I(\mathbf{R}^{(i)}(t))\rangle = \prod_n G_n^{(i)}(\mathbf{x},\mathbf{p};t)\exp\left[\frac{i}{\hbar} S^{(i)}[\mathbf{R}^{(i)}(t)]\right], \tag{16}$$

where

$$G_n^{(i)}(\mathbf{x},\mathbf{p};t)=\left(\frac{a_n}{\pi}\right)^{3/4}\exp\left[-\frac{a_n}{2}(\mathbf{x}_n-\mathbf{x}_n^{(i)}(t))^2+\frac{i}{\hbar}\mathbf{p}_n^{(i)}(t)\cdot(\mathbf{x}_n-\mathbf{x}_n^{(i)}(t))\right], \tag{17}$$

$\mathbf{R}^{(i)}(t)=\{\mathbf{x}_1^{(i)}(t),\mathbf{x}_2^{(i)}(t),\cdots\}$, and $\mathbf{x}_n^{(i)}(t)$ is the position of the nth nuclei, $\mathbf{p}_n^{(i)}(t)$ is the momentum of the nth nuclei and a_n is the Gaussian width of the nth nuclei (discussed further below). The phase evolution of the total wave function is given by the classical action, $S^{(i)}(t)$, of the system during propagation along state i which is given explicitly by

$$S^{(i)}[\mathbf{R}^{(i)}(t)]=\int_0^t dt\sum_n\frac{(\mathbf{p}_n^{(i)}(t))^2}{2M_n}-\langle I(\mathbf{R}^{(i)}(t))|H_i(t)|I(\mathbf{R}^{(i)}(t))\rangle. \tag{18}$$

The second term in Eq. (18) is simply the potential energy of the system on surface i evaluated for the position of the classical coordinates at time t. Since the frozen Gaussians are propagated classically, the quantum wave function of the bath is directly available from the semiclassical description of the entire system. Armed with Eq. (16) and Eq. (18), the nonadiabatic transition rate can be calculated using Eq. (6). This was the approach used by Neria and Nitzan, who calculated the nuclear overlap integral from Eq. (8) as[7,8]

$$J(t)\approx\left\langle\prod_m G_m^{(j)}(\mathbf{x}_m^{(j)},\mathbf{p}_m^{(j)};t)\middle|\prod_n G_n^{(i)}(\mathbf{x}_n^{(i)},\mathbf{p}_n^{(j)};t)\right\rangle\times\exp\left[\frac{i}{\hbar}(S^{(i)}[\mathbf{R}^{(i)}(t)]-S^{(j)}[\mathbf{R}^{(j)}(t)])\right] \tag{19}$$

by running two quantum adiabatic simulations from the same initial condition, one starting on the initial electronic surface and one starting on the final electronic surface. The drawback to this technique is that it requires running many costly adiabatic quantum molecular dynamics trajectories (two trajectories per configuration in the ensemble) simply to estimate the overall rate at the level of first order perturbation theory [Eq. (6)]. This effort is spent on trajectories which provide no dynamical information about the system. Instead, we can use Eq. (19) as a starting point to provide an estimate of the decoherence time that can then be used in either the stationary phase surface hopping or fewest switches molecular dynamics algorithms. Both algorithms furnish the dynamical information of interest, and further, the stationary phase surface hopping approach utilizes the full quantum propagator (within the stationary phase approximation) so that the assumption of linear coupling inherent in first order perturbation theory is not an issue.

The computational effort involved in Eq. (19), however, is formidable for the sole purpose of providing a single decoherence time for use in another algorithm. Since the FGA is an inherently short time approximation, a reasonable approach to reducing the computational effort in estimating the decoherence time is to expand the classical nuclear positions and momenta to second order in time. This is equivalent to making a local harmonic approximation for the classical motion, in accord with the original use of frozen Gaussians. This type of approximation can describe condensed phase dynamical properties for a surprisingly long period of time (certainly longer than the decoherence time of interest, discussed below), as demonstrated in the rapidly growing literature devoted to instantaneous normal mode (INM) analysis of classical liquids.[22] In general, the Gaussian overlap integral in Eq. (19) can be done analytically[21]

$$\begin{aligned}\left\langle\prod_m G_m^{(j)}(\mathbf{x}_m^{(j)},\mathbf{p}_m^{(j)};t)\middle|\prod_n G_n^{(i)}(\mathbf{x}_n^{(i)},\mathbf{p}_n^{(i)};t)\right\rangle&=\prod_n\exp\left[-\frac{a_n}{4}(\mathbf{x}_n^{(j)}(t)-\mathbf{x}_n^{(i)}(t))^2\right]\\&\times\exp\left[-\frac{1}{4a_n\hbar^2}(\mathbf{p}_n^{(j)}(t)-\mathbf{p}_n^{(i)}(t))^2\right]\\&\times\exp\left[\frac{i}{2\hbar}(\mathbf{x}_n^{(j)}(t)-\mathbf{x}_n^{(i)}(t))\cdot(\mathbf{p}_n^{(J)}(t)+\mathbf{p}_n^{(i)}(t))\right],\end{aligned} \tag{20}$$

where we have neglected the overlap of Gaussians representing different nuclei ($n\neq m$) between the two surfaces. The short time expansion for the nuclear degrees of freedom is given by

$$\begin{aligned}\mathbf{x}_n^{(i)}(t)&\approx\mathbf{x}_n^{(i)}(0)+\frac{1}{M_n}\mathbf{p}_n^{(i)}(0)t+\frac{1}{2M_n}\mathbf{F}_n^{(i)}(0)t^2+\mathcal{O}(t^3),\\\mathbf{p}_n^{(i)}(t))&\approx\mathbf{p}_n^{(i)}(0))+\mathbf{F}_n^{(i)}(0)t+\frac{1}{2M_n}\frac{\partial\mathbf{F}_n^{(i)}(0)}{\partial t}t^2+\mathcal{O}(t^3).\end{aligned} \tag{21}$$

In Eq. (21), $\mathbf{F}_n^{(i)}(0)=\mathbf{F}_{Q,n}^{(i)}(0)+\mathbf{F}_{\mathrm{Cl},n}(0)$, the sum of the quantum and the classical forces acting on the nth nucleus at time zero, where $\mathbf{F}_{Q,n}^{(i)}(0)$ is the adiabatic (Hellmann–Feynman) quantum force acting on nucleus n when the quantum state is on surface i as given by Eq. (12). Also needed is a short time expansion for the potential energy term in the classical action, Eq. (18), which enters into phase of the total nuclear wave function

$$\begin{aligned}V^{(i)}(\mathbf{R}(t))&=\langle I(\mathbf{R}^{(i)}(t))|H_i(t)|I(\mathbf{R}^{(i)}(t))\rangle\\&\approx V^{(i)}(\mathbf{R}(0))+t\sum_n\frac{\mathbf{p}_n^{(i)}(0))}{M_n}\cdot\mathbf{F}_n^{(i)}(0)+\cdots,\end{aligned} \tag{22}$$

where we have used the chain rule for differentiation to get the second term in the expansion.

In general, $J(t)$ is a complex-valued function of time. Utilizing the Condon approximation, where we assume that the value of $J(t)$ is uncorrelated with the instantaneous value of the nonadiabatic coupling vector, we can separate the contribution of $J(t)$ from the overall golden rule expression, Eq. (6). Since the imaginary part of $J(t)$ is odd with respect to time, we need only consider the real part of $J(t)$ in our estimate of the quantum decoherence time and its effect on the non-adiabatic transition rate. We also note that the golden

rule expression requires that the trajectories used to determine the classical coordinates propagated on the two electronic surfaces start from the same set of initial conditions[8] $\mathbf{x}_n^{(i)}(0)=\mathbf{x}_n^{(j)}(0)$, $\mathbf{p}_n^{(i)}(0)=\mathbf{p}_n^{(j)}(0)$, which also means that the initial classical forces acting on nucleus n are the same on the two surfaces. Using this information, substituting Eqs. (20)–(22) into Eq. (19), and dropping terms of $\mathcal{O}(t^3)$ and higher, we have the desired short-time approximation for the decay of quantum coherence

$$\mathrm{Re}[J(t)]=\exp\left[-\sum_n \frac{1}{4a_n\hbar^2}(\boldsymbol{F}_{Q,n}^{(i)}(0)-\boldsymbol{F}_{Q,n}^{(j)}(0))^2t^2\right]\times\cos[(V^{(i)}(\mathbf{R}(0))-V^{(j)}(\mathbf{R}(0)))t/\hbar]. \quad (23)$$

The exponential term in Eq. (23) arises from the divergence in nuclear overlap for propagation on the two different surfaces. The time derivative of the quantum force in the short time expansion for the momentum [Eq. (21)] and the $\mathbf{x}\cdot\mathbf{p}$ terms from Eq. (20) both come in at higher order than t^2, and hence do not appear in Eq. (23). Further, because the initial positions and momenta are the same on the two surfaces, the leading term in the divergence of the overlap comes in only as the difference in the quantum forces evaluated on the two adiabatic surfaces. The cosine term in Eq. (23) arises from the classical action; the term which survives depends only on the potential difference between the two states since the initial classical kinetic energy is the same on both surfaces. Finally, although the nuclear masses do not appear explicitly in Eq. (23), they will play an implicit role in decoherence through the choice of the Gaussian widths, a_n. Thus the decoherence time as given by the decay of $J(t)$ in Eq. (23) depends upon the initial width of the Gaussians. As is clear from Eq. (23), the solvent nuclear dynamics enters only through the force difference. It is also interesting to note that it is the dispersion of the *momentum* components of the nuclear wave function which governs the initial decay of $J(t)$ rather than the spatial components.

Our short time approximation for $J(t)$ in Eq. (23), depends solely on zero time quantities, a substantial advantage over a time dependent expression. For a given nuclear configuration, only the potential energy difference of the quantum system and the difference in the adiabatic quantum force on the two surfaces play a role in determining the decoherence time. Since $J(t)$ is defined for a single configuration, it can be computed on the fly during nonadiabatic dynamics to monitor the non-equilibrium evolution of quantum decoherence.[23] For the equilibrium ensemble case, initial nuclear configurations can be generated from a single adiabatic mixed quantum-classical trajectory on the initial surface or by Monte Carlo, with no need to run multiple trajectories for each member of the ensemble. In the common situation where the initial configurations are generated by molecular dynamics, the potential energy difference is typically known and the Hellmann–Feynman force has already been computed on the occupied surface, so the only additional computation necessary is determination of the quantum force on the final electronic surface. Although the formalism presented here considers decoherence between only two quantum states, generalization to an arbitrary number of pairs of states is completely straightforward. We offer an example of the utility of this new method for estimating the decoherence time in the following section.

IV. QUANTUM DECOHERENCE AND THE HYDRATED ELECTRON

The prototypical system for studying condensed phase nonadiabatic dynamics has been the hydrated electron. Because it has only one quantum (electronic) degree of freedom which is strongly coupled with the nuclear motions of the surrounding bath, the hydrated electron provides an excellent testing ground for theoretical models.[7,8,10,13,23–29] The large optical cross section of the hydrated electron also makes it amenable to spectroscopic investigation.[30–36] With the advent of new femtosecond laser techniques and the development of nonadiabatic dynamical algorithms such as those described above, the hydrated electron has provided the first condensed system where nonadiabatic theory and experiment have successfully converged.[37]

Interest in the nonadiabatic dynamics of the hydrated electron was originally spurred by femtosecond experiments studying the formation of equilibrium hydrated electrons following multiphoton ionization of neat water.[32,33] While the mechanism of electron production in these experiments is not fully understood,[35,36] it is clear that the formation of the equilibrium species takes place by an essentially two-state process. The kinetic picture[28] that emerged from the combination of these experiments,[32,33] adiabatic simulations,[29] and nonadiabatic calculations[13,26] points to trapping of the electron in the lowest excited state (sometimes referred to as the ''wet'' electron) followed by nonadiabatic relaxation to the ground state (the equilibrium ''solvated'' electron). Formation of the excited state electron from the initially produced species was found to take 110–240 fs.[32,33] The nonadiabatic relaxation time for the electron determined in these experiments is 250–500 fs.[32,33] Investigations of this process in deuterated water have shown that the isotope effect on the nonadiabatic transition rate is at most a few percent.[34]

More recent experiments[30,31] and quantum simulations[10,24,25,27] have investigated the nonadiabatic dynamics of the hydrated electron by photoexciting the equilibrium ground state species and monitoring the subsequent solvation of the excited state and its internal conversion back to the ground state. Upon photoexcitation, the quantum energy gap of the hydrated electron starts at its equilibrium ground state value and continuously decreases with time as the excited state charge distribution is solvated. The nonadiabatic coupling between the two states increases as the gap becomes smaller, leading to an increasing nonadiabatic transition rate with time.[24] The excited state solvation time for the photoexcited electron is 250–300 fs, and the nonadiabatic transition rate from the equilibrated excited state is on the order of 1 ps^{-1}.[24,30] Experiments in D_2O show identical spectral dynamics, indicating little isotope effect on either the solvation dynamics or the nonadiabatic transition rate.[30] Here, we utilize nonadiabatic mixed quantum-classical molecular dynam-

ics simulations to investigate the origins of quantum decoherence in this prototypical condensed phase system.

The simulation techniques we employ are identical to our earlier work studying both the relaxation of electrons photoinjected into neat water[13,26] as well as the present case of photoexcitation of equilibrium hydrated electrons.[24,25] Briefly, the model consists of 200 classical SPC water molecules with the addition of internal flexibility[38] and one quantum electron in a cubic cell of side 18.17 Å (corresponding to a solvent density of 0.997 g/ml) with standard periodic boundary conditions at room temperature. The electron–water interactions were described with a pseudopotential,[39] and the equations of motion integrated using the Verlet algorithm with a 1 fs time step in the microcanonical ensemble.[40] The adiabatic eigenstates at each time step were computed via an efficient iterative and block Lanczos scheme utilizing a 16^3 plane wave basis;[13] the lowest six eigenstates were computed during nonadiabatic molecular dynamics. Twenty configurations in which the energy gap was resonant with the experimental laser frequency[24,30] were chosen from a 35 ps equilibrated ground state run as the starting points for nonequilibrium excited state trajectories. The solvation of the newly formed excited state, nonadiabatic transition times for the 20 trajectories, and a comparison of ultrafast spectroscopy computed from these simulations to experiment are all available in the literature.[24,25] A detailed microscopic analysis of the nonadiabatic coupling and energy disposal following the internal conversion for these simulations is forthcoming.[41]

Quantum coherence in these simulations was maintained utilizing the stationary phase surface hopping nonadiabatic dynamics algorithm of Webster *et al.*, described above.[13,14] In these earlier studies of the hydrated electron, we chose to drop coherence at the end of each 1 fs time step (in other words, we do not utilize the complex phases of the transition amplitudes, T_{ij} [Eq. (15)], over more than one time step). This choice, though arbitrary, was based on expectations that the decoherence time for this system should be on the order of 1 fs. This choice is equivalent to having a rectangular decay of the nuclear function $J(t)$ [Eq. (23)]: $J(t)$ for this algorithm starts at 1 and stays there for 1 fs, and then instantly drops to zero for times greater than 1 fs. A modified version of this algorithm which chooses coherence intervals based on instantaneous values for the quantum decoherence time will allow for dynamics with a more realistic decay of quantum coherence.[23] The rapid divergence of the nuclear positions on the two different surfaces (and hence, choice of a short coherence time) is illustrated conceptually by Fig. 1. This figure shows the quantum energy gap for the hydrated electron starting from a configuration equilibrated on the electronic excited state. The solid curve follows the energy gap for continued propagation on the equilibrium excited surface, while the dashed curve shows the gap starting from the same initial configuration but propagating along the ground state surface. Clearly the nuclear configurations giving rise to the quantum energy gap on the different surfaces must diverge rapidly. Thus the nonadiabatic coupling for this system must be tempered by a short coherence time.

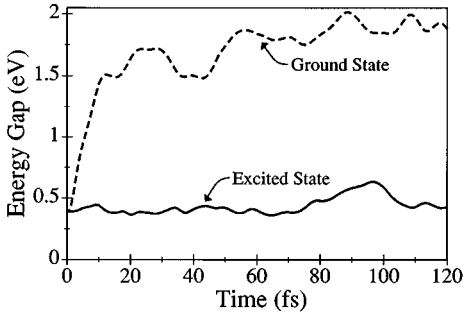

FIG. 1. Divergence of the ground state-excited state energy gap of the hydrated electron for trajectories propagating on the ground versus excited state potential surfaces, starting from the same initial configuration in the equilibrated excited state. The solid curve indicates that continued propagation along the excited state produces little change in the quantum energy gap (Ref. 43). The dashed line shows the rapid increase in the quantum energy gap as the electron propagates on the ground state surface, establishing its new equilibrium.

Using the method outlined in the previous section, we can estimate the decay of quantum coherence for the hydrated electron from Eq. (23) with information available from the excited state simulations. For the present example, the initial state i is the equilibrium excited state of the hydrated electron, and the final state j is the ground state of the electron. For the widths of the frozen Gaussians, we chose

$$a_n = \frac{6M_n kT}{\hbar^2} \tag{24}$$

which results from rigorous analysis of the nonadiabatic transition rate between displaced harmonic oscillators in the high temperature limit,[7,8] and also allows for direct comparison to the earlier calculations of Neria and Nitzan.[7,8] To compute the equilibrium quantum decoherence which modulates the nonadiabatic transition from the excited state, we take an ensemble average of Eq. (23). Assuming that the excited state was equilibrated at times past 1 ps, we chose 20 configurations at 25–50 fs intervals from each of our 5 longest trajectories for a total of 100 configurations. Since we had already computed the eigenenergies and the excited state Hellmann–Feynman forces on the classical particles for all these configurations, we need only use the eigenfunctions computed previously to determine the Hellmann–Feynman forces along the ground state [Eq. (12)] to obtain an estimate of $J(t)$ from Eq. (23).

The results of this calculation are shown as the solid curve in Fig. 2. For the hydrated electron in the short time approximation, the coherence decays in a roughly Gaussian manner, and a Gaussian fit to the decay has a variance of 3.1 fs. Another estimate of the decoherence time is found in the area under the curve, which for this example is 2.8 fs. This result is in good agreement with previous calculations using a different model for the hydrated electron,[7,8] and demonstrates *a posteriori* justification for the hypothesis of a $\approx$1 fs coherence time in the earlier nonequilibrium simulations. We also note that the rapid decoherence of this system provides *a posteriori* justification for the short time approximations

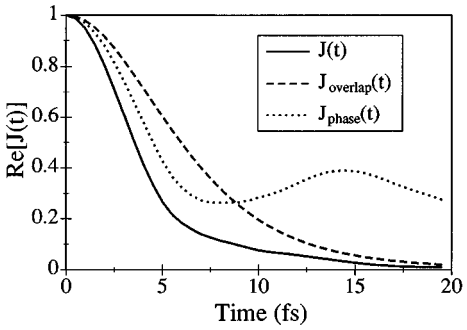

FIG. 2. The decay of quantum coherence for the hydrated electron in the short time approximation. The solid curve shows the full decay of coherence due to divergent nuclear overlap and phases on the two different surfaces [Eq. (23)]. The dotted curve shows the portion of the coherence decay due solely to the difference in nuclear phases [Eq. (24)]. The dashed curve presents the contribution of the decaying overlap of the diverging nuclear positions to the decay of quantum coherence [Eq. (25)]. The product of the phase and overlap terms does not exactly reproduce the full coherence decay due to correlation between them.

[Eqs. (21) and (22)] inherent in Eq. (23). Since the computed decoherence time is on the order of a few femtoseconds, Eq. (23) should prove to be an excellent approximation. The importance of the coherence decay in the overall rate is evident from Eq. (6): $J(t)$ decays much more quickly than the autocorrelation of the nonadiabatic coupling.[41] The origins of the coherence decay presented in Fig. 2 can be found in a detailed examination of Eq. (23). The dashed curve in Fig. 2 shows the ensemble average of only the Gaussian term in Eq. (23), namely,

$$J_{\text{overlap}}(t)=\left\langle \exp\left[-\sum_n \frac{(\boldsymbol{F}_{Q,n}^{(i)}(0)-\boldsymbol{F}_{Q,n}^{(j)}(0))^2}{4a_n\hbar^2}\,t^2\right]\right\rangle. \tag{25}$$

This portion of the decoherence, due to the decay in overlap of the nuclear wave function on the different surfaces, decays more slowly than the total coherence indicating the importance also of the phase of the nuclear wave function (see below). We find that the sum in the exponential is typically dominated by only 5 to 10 nuclei which are the closest to the bulk of the electronic charge density.[42] This makes sense from the definition of the Hellmann–Feynman force, Eq. (12): The largest difference in quantum force between the two surfaces will be for nuclei in positions where the charge density, is large on one surface and small on the other. We find that despite the appearance of the nuclear mass in the Gaussian width [Eq. (24)], not only hydrogen (deuterium) but also occasionally oxygen nuclei contribute significantly to the sum representing the decay of the nuclear overlap [Eq. (25)]. This is due to the fact that the force difference between adiabatic energy surfaces for O nuclei can sometimes be larger than that for H nuclei. This larger force difference relative to the H nuclei results from the larger charge on the O atoms which increases the difference in Coulomb forces, and from the larger O atom electron density which increases the difference in Pauli repulsion forces. These contributions, taken together, can be large enough to overcome the mass weighting which favors contributions from H atoms.

The dotted curve in Fig. 2 shows the portion of the coherence decay due to the ensemble average of the cosine term in Eq. (23)

$$J_{\text{phase}}(t)\approx\langle\cos[(V^{(i)}(\mathbf{R}(0))-V^{(j)}(\mathbf{R}(0)))t/\hbar]\rangle. \tag{26}$$

This portion of the total coherence, due to phase interferences in the nuclear part of the total wave function associated with the two electronic surfaces, accounts for a significant portion of the total decoherence of the system. For the hydrated electron, the distribution of initial potential energy differences is large[43] leading to cosine terms from the nuclear phases of a wide variety of frequencies which destructively interfere. We also note that the product of the individually averaged overlap and phase terms, Eqs. (25) and (26), does not exactly yield the total coherence decay calculated from Eq. (23). This indicates a definite correlation between the overlap and phase portions of the nuclear wave function. Such correlation is perhaps not that surprising: Configurations with larger potential energy differences are also more likely to have larger differences in quantum forces between the two surfaces.

Finally, we note that the decay of quantum coherence presented in Fig. 2 is calculated for the hydrated electron at equilibrium in its excited state. Since the quantum energy gap evolves with time following photoexcitation due to solvation, the decay of quantum coherence will likely also evolve during the course of a nonequilibrium trajectory. Thus dynamical changes in both the nonadiabatic coupling and the quantum decoherence time will affect the nonadiabatic transition rate during solvation of the newly created excited state. For now, we will concentrate solely on the nonadiabatic transition rate from the equilibrated excited state; the effects of evolving decoherence on condensed phase nonadiabatic dynamics will be explored elsewhere.[23]

V. DECOHERENCE AND THE ISOTOPE EFFECT ON NONADIABATIC TRANSITION RATES

One of the largest puzzles concerning the nonadiabatic dynamics of the hydrated electron has been the surprising lack of a sizable isotope effect on the radiationless transition rate.[30,34] A quick glance at Eq. (6) shows that the nuclear velocities play a direct role in determination of the nonadiabatic transition rate. Since the fastest nuclear velocities in D_2O are classically $\sqrt{2}$ times slower than those in H_2O while the other factors (the electron–water interaction potential, the quantum force on the nuclei, etc.) remain the same between the two solvents, the expectation is that radiationless transition rates should be roughly half as large in D_2O compared to H_2O. Indeed, mixed quantum-classical simulations have suggested isotope effects of factors of 2–4 for the electronic transition rate in this system.[7,8,44] Experiments, however, have found at most a modest difference in the nonadiabatic transition rate for electrons photoinjected into H_2O vs D_2O,[34] and no isotopic differences have been observed in the

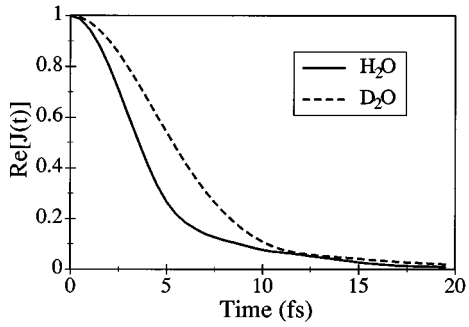

FIG. 3. The isotope effect on quantum decoherence. The solid line shows the full decay of quantum coherence for the hydrated electron [Eq. (23)], same as the solid line in Fig. 2. The dashed line shows the full decay of quantum coherence for the solvated electron in D_2O. The isotope effect slows the coherence decay in heavy water by ≈50%; see the text for details.

spectroscopic dynamics for photoexcited equilibrium electrons.[30] In this section, we explore the possible role of quantum coherence in determining the magnitude of the nonadiabatic transition rate for equilibrium excited state electrons. We find that even though the nonadiabatic coupling is smaller in D_2O than H_2O, a slower decay of quantum decoherence in D_2O allows this smaller coupling to add coherently for a longer time than in H_2O, leading to estimated net electronic transition rates which are comparable in the two solvents.

The simulation techniques we have employed to study the solvated electron in D_2O are essentially identical to those in H_2O, and are described in more detail elsewhere.[44] Briefly, the only differences in simulating the electron in heavy versus light water come in changing the mass of the proton from 1 to 2 amu, and the slight change in solvent density to accurately reflect the experimental density of D_2O at room temperature. In performing these D_2O simulations, carried out prior to the remainder of the present study, we made the choice of a quantum coherence time in the stationary phase surface hopping algorithm of 1 fs, the same as for H_2O. As we will see below, the estimated coherence time in D_2O is roughly 50% longer than that in H_2O. One of the consequences of the hypothesis of equal coherence times is that nonadiabatic trajectories remain on the excited state significantly longer in D_2O, bringing to light a slower component of the solvation response on the ≈1.2 ps time scale that was not evident in our earlier work[24,25] on H_2O due to its shorter excited state lifetime.[44] For consistency in estimating the coherence decay by use of Eq. (23), we chose 100 excited state configurations from the D_2O trajectories at the same times ($\geqslant$1 ps) that we used for the H_2O trajectories in the production of Fig. 2.

Figure 3 shows a comparison of the nuclear decay function $J(t)$ for the solvated electron in H_2O (solid curve, same as the solid curve in Fig. 2) and in D_2O (dashed curve), calculated from Eqs. (23) and (24). The coherence decay in D_2O is qualitatively similar to that in H_2O, only for D_2O the approximate Gaussian decay time is ≈4.6 fs (versus ≈3.1 fs for H_2O) and the area under the curve is 4.1 fs (vs 2.8 fs for H_2O). We note that the results in this figure are not in good agreement with the previous work of Neria and Nitzan,[7,8] who found almost identical coherence decays for the electron in H_2O and D_2O.[45] Although we cannot be sure, the difference may reflect the result of statistical fluctuations in Neria and Nitzan's data. To evaluate the nonadiabatic transition rate, Neria and Nitzan utilized Eq. (6) which requires running trajectories on both electronic surfaces. Since such trajectories are costly, they limited their ensemble to only 15 examples.[7,8] With our short time approximation, we were able to easily include 100 examples in the determination of the coherence decay. When we mimicked their calculation by selecting different subsets of only 15 examples for the ensemble average, we found coherence decays that varied by nearly a factor of 3. This suggests that insufficient statistics may have played a role in Neria and Nitzan's result of identical coherence decays for the two fluids. We note that, correspondingly, Ref. 8 reports a substantially different isotope effect than we report below.

The longer coherence time in heavy water compared to light water arises predominantly from the difference in mass in the choice of the Gaussian width [Eq. (24)]. For classical H_2O and D_2O, the probability of a given nuclear configuration is the same. Static ensemble properties for the two fluids should be identical since the ensembles contain identical nuclear configurations with equal statistical weights.[46] Since the electronic Hamiltonian for the solvated electron is identical for both heavy and light water, the static ensemble averaged potential energy difference and the difference in Hellmann–Feynman forces on the two surfaces will also be identical for the two fluids. Thus the only differences in the evaluation of the coherence decay for the two fluids via Eq. (23) is in the mass term that enters through the Gaussian width in Eq. (24). Since the nuclear overlap part of the coherence decay depends on the sum over nuclei, the mass change leads to the net slower decay of coherence in D_2O vs H_2O. In fact, for the purposes of evaluating $J(t)$ for the solvated electron in D_2O, the H_2O simulations would suffice.

The different coherence decay times in the two solvents play a direct role in determining the isotope effect on the overall nonadiabatic transition rate. In simplified terms, to determine the nonadiabatic transition rate before quantum coherence has decayed, nonadiabatic transition *amplitudes* should be added; after the decoherence interval, memory of the complex phases is lost and nonadiabatic transition *probabilities* should be added. This view can be used to estimate nonradiative transition rates in limiting cases. During the course of the nonadiabatic simulations described above, the probability of making an electronic transition at a given time step was strictly determined by the square of the appropriate nonadiabatic transition amplitude, a direct consequence of the choice to keep coherence for only one time step. Thus the nonadiabatic transition rate, or probability of making the transition per unit time in this ''incoherent'' limit, is given by the sum of the squares of the nonadiabatic transition amplitudes

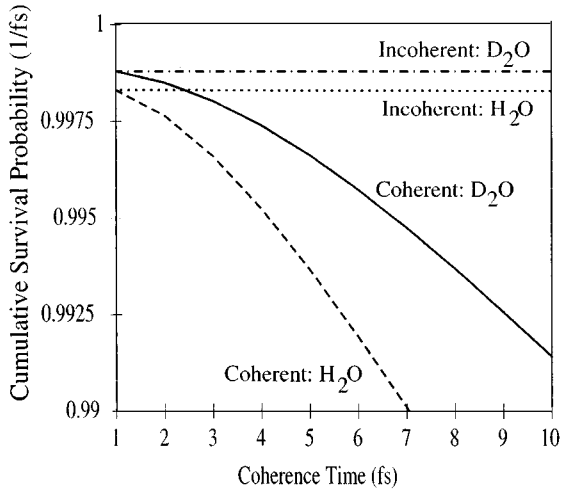

FIG. 4. Effect of quantum decoherence on the survival probability per unit time of the hydrated electron. The dashed and dot–dashed lines show the incoherent limit [Eq. (27)] to remain in the excited state for the solvated electron in light and heavy water, respectively. Since the average probability for making a transition is constant, these incoherent sums do not change with time. The dashed and solid curves show the corresponding coherent products of the nonadiabatic transition amplitudes [Eq. (28)] in light and heavy water, respectively. The coherent and incoherent transition probabilities are identical for 1 fs coherence time due to the simulation algorithm.

$$P_{ij}(\Delta t)=\frac{1}{\Delta t}\left\langle \sum_{n=1}^{\tau}\left|T_{ij}(\Delta t)\right|^2\right\rangle. \tag{27}$$

In Eq. (27), $P_{ij}(\Delta t)$ is the probability per unit time of making a nonadiabatic transition between states i and j averaged over τ time steps along a trajectory in the limit of keeping coherence for only one time step (Δt). The τ consecutive transition amplitudes, $T_{ij}(\Delta t)$, are given by Eq. (15), and the angled brackets indicate an ensemble average over starting times and trajectories. If coherence were maintained over several consecutive time steps $(\tau=n\Delta t)$, the complex transition amplitudes would first be summed over those time steps, allowing for interference, and then the square would be taken to determine the nonadiabatic transition probability

$$P_{ij}(\tau)=\frac{1}{\tau}\left\langle \left|\sum_{n=1}^{\tau}T_{ij}(n\Delta t)\right|^2\right\rangle. \tag{28}$$

In Eq. (28), $P_{ij}(\tau)$ is the probability of making a nonadiabatic transition between states i and j per unit time where coherence is completely maintained for τ consecutive time steps [$T_{ij}(n\Delta t)$ is the nonadiabatic transition amplitude at the nth time step]. Thus the complex transition amplitudes from the simulation can be used after the fact to determine what the nonadiabatic transition rate would have been if quantum coherence were retained over an arbitrary number of time steps. Comparison of nonadiabatic transition probabilities determined from Eqs. (27) and (28) as a function of τ provides a direct measure of the influence of coherence on nonadiabatic transition rates.

Figure 4 displays the nonadiabatic transition probability for remaining in the equilibrium excited state, P_{22}, computed as a function of the coherence time for the solvated electron in both H_2O and D_2O. The dotted and dot–dashed lines show the average probability per unit time for the electron to remain on the excited state in light and heavy water, respectively, as computed during the simulations with a 1 fs quantum coherence time [$P_{22}(\Delta t)$, Eq. (27)]. These probabilities are averaged over 3000 starting configurations drawn from the 5 longest trajectories at times past 1 ps. The average probability per unit time of leaving the excited state for the electron in D_2O is approximately 1.2 parts per thousand while that for the hydrated electron is roughly half again as large. For a 1 fs time step, these average probabilities correspond to lifetimes of $\approx$550 fs in H_2O and $\approx$850 fs in D_2O. The magnitudes of these rates agree reasonably with the rates obtained from fits to the actual population decays in the simulations,[47] and the $\approx$2:1 simulated isotope effect between D_2O and H_2O[44] is adequately reproduced. As discussed elsewhere, non-adiabatic transitions usually occur from those configurations with somewhat higher than average transition probabilities or lower than average survival probabilities.[41] These special configurations, however, occur with a low enough frequency that the average transition probability provides a reasonable estimate of the nonequilibrium population dynamics.

The solid and dashed curves in Fig. 4 show the average probability per unit time for remaining in the excited state for the solvated electron in heavy and light water, respectively, computed as a function of the coherence time τ [$P_{22}(\tau)$, Eq. (28)]. For a coherence time $\tau=1$ fs, these curves coincide exactly with those computed from Eq. (27), as expected. For coherence times longer than 1 fs, constructive interference between the transition amplitudes at consecutive time steps leads to a significant lowering of the survival probability per unit time—in other words, increasing the quantum coherence time increases the likelihood for making a nonadiabatic transition. The magnitude and phase of the nonadiabatic coupling in this system do not vary much on the time scale of a few femtoseconds, so that changes in the coherence time result directly in changes in the electronic transition rate as per Eq. (6).

Armed with the coherence decay times for both H_2O and D_2O from Fig. 3, we can make use of the coherence time dependence of the nonadiabatic transition probabilities per unit time displayed in Fig. 4 to provide a revised estimate of the isotope effect on the nonadiabatic transition rate. For equal coherence decay times, as per the original ansatz in the simulations, the survival probabilities in Fig. 4 predict a roughly 2:1 isotope effect in the nonadiabatic transition rate between D_2O and H_2O. This is a direct reflection of smaller nonadiabatic coupling in D_2O due to smaller nuclear velocities. However, for a decoherence time in D_2O which is roughly 50% longer than that in H_2O (we could chose either the $\approx$4.6 fs vs $\approx$3.1 fs Gaussian decay times or the 4.1 fs vs 2.8 fs areas under the curves in Fig. 3), the present method of estimation yields nonadiabatic transition rates in the two solvents which are identical to within 10%. For example, choosing the areas under the $J(t)$ curves as estimates of the decoherence times, we obtain predicted lifetimes for the

equilibrium excited state of the solvated electron of 310 and 345 fs in H_2O and D_2O, respectively (cf. Fig. 4). This result provides a microscopic explanation for the lack of isotope effect observed in the femtosecond experiments: The smaller nonadiabatic coupling in D_2O adds coherently for a longer time than that in H_2O; the two opposing effects nearly cancel for this system, leading to a nonintuitively small isotopic dependence of the nonadiabatic transition rate.[48] Although the absolute transition rate constants are difficult to predict from simulation,[49] Fig. 4 provides a clear demonstration that quantum decoherence plays a direct role in the electronic dynamics of this very important condensed phase chemical system.

VI. CONCLUSIONS

In summary, we have investigated the role of quantum decoherence in condensed phase nonadiabatic chemical reactions. In mixed quantum-classical computer simulations, basic assumptions about the decoherence time produce direct manifestations on the calculated nonadiabatic dynamics, and hence play an important role in understanding a wide variety of chemical systems. The treatment of quantum coherence can be formulated somewhat differently in the two types of nonadiabatic algorithms we explored. In Tully's fewest switches method,[6,12] the complex phases of the nonadiabatic transition amplitudes are retained at all time steps, so that the dynamics of individual trajectories are completely coherent. Decoherence can then treated by running a swarm of trajectories from the same initial condition, so that the amplitudes added between trajectories which underwent switches at different times can destructively interfere. In the stationary phase surface hopping method of Webster *et al.*,[13–15] mixed quantum classical dynamics are performed coherently for a single time step using a semiclassical expression based on the stationary phase approximation for the quantum force. The complex transition amplitudes can then be added coherently over any number of time steps, providing an arbitrary decoherence time in a single trajectory. A recently developed extension of the fewest switches algorithm[5] will provide for a smooth decay of quantum coherence, with the coherence decay time used as an input parameter. Alternatively, modification of the stationary phase surface hopping method using the formalism outlined here will allow for computation of the decoherence time on the fly during the course of a nonadiabatic trajectory.[23]

In the formalism of time-dependent perturbation theory, the nonadiabatic transition rate for a condensed phase system can be written as the integral of the autocorrelation of the nonadiabatic coupling vector modulated by the decay of quantum coherence [Eq. (6)].[7,8] By building a short time approximation into a semiclassical golden rule method developed by Neria and Nitzan which utilizes frozen Gaussians[21] to approximate the nuclear wavefunction of the bath,[7,8] we developed a readily computable way to evaluate the desired value for the rate of the decay of quantum coherence in the condensed phase [Eq. (23)]. The method has the advantage that the decoherence time can be estimated simply from knowledge of the difference in quantum forces and the difference in potential energy between the two states involved in the nonadiabatic transition, requiring only a single quantum trajectory or a set of configurations generated by Monte Carlo. Application of this new method to the hydrated electron reveals that the decay of quantum coherence takes place because of destructive interference in the phases of the total bath wave functions as well as in the decay of the nuclear overlaps in the bath wave functions as the nuclear dynamics diverge on alternative surfaces.

An important test of the effects of quantum decoherence on nonadiabatic dynamics is found in an examination of the isotope effect on the internal conversion rate of the hydrated electron. Ultrafast spectroscopic experiments studying both the formation of ground state electrons following multiphoton ionization and the internal conversion dynamics of photoexcited equilibrium ground state electrons find little or no evidence for an isotope effect in the nonadiabatic dynamics of this system.[30,34] The decay of quantum coherence for the solvated electron evaluated by the expression developed here is found to be 50% longer in D_2O than in H_2O, predominantly due to effects of the nuclear mass on the total wave function of the bath. This difference in the decoherence time has been shown to provide an explanation for the observed lack of isotope effect. Since the autocorrelation of the nonadiabatic coupling decays relatively slowly for this system, increasing the decoherence time allows the coupling to add coherently for longer times, leading to an increase in the nonadiabatic transition rate. The longer decoherence time in D_2O compared to H_2O balances the effect of the smaller nonadiabatic coupling due to the smaller nuclear velocities. As a result, the net nonadiabatic transition rate in the two solvents is nearly identical.

This dependence of the nonadiabatic transition rate on the quantum decoherence time has important implications for a variety of chemical reactions. There are many chemical systems in which a bath is coupled to a quantum coordinate of interest: internal conversion and internal vibrational energy redistribution in isolated molecules (here, the bath is comprised of all the modes of the molecule but the one of interest); electronic energy transfer between molecules or different parts of the same molecule; and charge transfer reactions including proton and electron transfer. In these latter examples, both the condensed environment and other modes in the molecules can act as the bath which couples the states together. The decay of quantum coherence, which depends on the frequencies and populations of the bath modes coupled to any of the above systems, will determine the extent to which the nonadiabatic coupling can act to allow the chemical reaction to proceed. Changes in the decoherence time due to variations in temperature or isotopic substitution can thus have a substantial impact in nonadiabatic chemical dynamics; the decay of quantum coherence can determine the degree of adiabaticity for a chemical reaction.[3]

Nowhere is the sensitivity of chemical reactions to the degree of adiabaticity more evident than in electron transfer reactions.[50,51] Since many important electron transfer reactions are highly nonadiabatic, small changes in the degree of

adiabaticity due to variations in the decoherence time will lead to large changes in the electron transfer rate. Using a modified version of the fewest switches algorithm, the role of decoherence was recently explored using a simple model of coupled displaced harmonic oscillators which represents an electron transfer reaction.[5] Indeed, changing the decoherence time in this type of system leads to dramatic differences in nonadiabatic rate constants and the overall population dynamics for the system.[5] Given that the effects of quantum decoherence can also lead to surprising results, exemplified by the lack of and isotope effect on the relaxation of the hydrated electron, the role of decoherence in chemical dynamics should not be underestimated. The methods outlined in this paper provide a practical starting point for explicitly incorporating decoherence in mixed quantum-classical descriptions of nonadiabatic chemical systems.

ACKNOWLEDGMENTS

This work was supported by the National Science Foundation. B.J.S. and E.R.B. gratefully acknowledge the support of National Science Foundation Postdoctoral Fellowships in Chemistry. B.J.S. thanks Bill Miller and David Chandler for stimulating conversations. We also wish to acknowledge Daniel Borgis for stimulating thoughts regarding the origin of the isotope effect, many of which motivated this work.

[1] The literature on mixed-quantum classical molecular dynamics simulations is enormous. We cite only a few recent examples here: A. Staib, D. Borgis, and J. T. Hynes, J. Chem. Phys. **102**, 2487 (1995); J. M. Papanikolas, P. E. Maslen, and R. Parson, *ibid*. **102**, 2452 (1995); Some recently developed adiabatic methods include: D. Thirumalai, E. J. Bruskin and B. J. Berne, J. Chem. Phys. **83**, 230 (1985); A. Selloni, R. Car, M. Parinello, and P. Carnevali, J. Phys. Chem. **91**, 4947 (1987); M. Sprik and M. L. Klein, J. Chem. Phys. **89**, 1592 (1988).

[2] There has also been a great deal of discussion of nonadiabatic dynamical algorithms and their importance to chemical reaction dynamics in the literature, which we make no attempt to review here. See, for example, the review by D. F. Coker, in *Computer Simulations in Chemical Physics*, edited by M. P. Allen and D. J. Tildesley (Kluwer Academic, Dordrecht, 1993), p. 315 and references therein. For a few recent examples of nonadiabatic dynamical calculations, see S. Hammes-Schiffer and J. C. Tully, J. Phys. Chem. **99**, 5793 (1995); L. Xiao and D. F. Coker, J. Chem. Phys. **102**, 1107 (1995) as well as Refs. 22–24.

[3] For a discussion of quantum coherence and adiabaticity in the condensed phase, see, for example, P. G. Wolynes, J. Chem. Phys. **86**, 1957 (1987).

[4] We note that the quantum decoherence time presented here is not trivially related to the spectroscopic dephasing time, which is generally taken to be a measure of the fluctuations in the energy gap of the quantum system. However, we note that the two quantities are rigorously identical in the limit when the quantum system is coupled linearly to a harmonic bath. For more details on electronic dephasing in the hydrated electron system, see S. J. Rosenthal, B. J. Schwartz, and P. J. Rossky, Chem. Phys. Lett. **229**, 443 (1994).

[5] E. R. Bittner and P. J. Rossky, J. Chem. Phys. **103**, 8130 (1995), and references therein.

[6] D. F. Coker and L. Xiao, J. Chem. Phys. **102**, 496 (1995), and references therein.

[7] E. Neria, A. Nitzan, R. N. Barnett, and U. Landmann, Phys. Rev. Lett. **67**, 1011 (1991).

[8] E. Neria and A. Nitzan, J. Chem. Phys. **99**, 1109 (1993).

[9] E. Neria and A. Nitzan, Chem. Phys. **183**, 351 (1994).

[10] A Staib and D. Borgis, J. Chem. Phys. **103**, 2642 (1995). This paper describes a semiclassical golden rule approach to nonadiabatic transition rates which captures elements of the quantum statistics of the bath.

[11] J. C. Tully and R. K. Preston, J. Chem. Phys. **55**, 562 (1971).

[12] J. C. Tully, J. Chem. Phys. **93**, 1061 (1990).

[13] F. A. Webster, J. Schnitker, M. S. Friedrichs, R. A. Friesner, and P. J. Rossky, Phys. Rev. Lett. **66**, 3172 (1991); F. A. Webster, P. J. Rossky, and R. A. Friesner, Comput. Phys. Commun. **63**, 494 (1991).

[14] F. A. Webster, E. T. Wang, P. J. Rossky, and R. A. Friesner, J. Chem. Phys. **100**, 4835 (1994).

[15] T. H. Murphrey and P. J. Rossky, J. Chem. Phys. **103**, 6665 (1995).

[16] See, for example, C. Cohen-Tannoudji, B. Diu, and F. Laloë, *Quantum Mechanics* (Wiley Interscience, New York, 1977).

[17] M. Gell-Mann and J. B. Hartle, Phys. Rev. D **47**, 3345 (1993); M. Gell-Mann and J. B. Hartle, in *Complexity, Entropy, and the Physics of Information*, edited by W. Zurek, SFI Studies in the Sciences of Complexity, Vol. VIII (Addison-Weseley, Reading, 1990).

[18] If there is not enough energy available in the classical coordinates along the nonadiabatic coupling vector to make up for the change in electronic energy, the transition is rejected. As pointed out in Ref. 8, near threshold for a transition, this ''rejection'' feature of the algorithm leads to a branching ratio between trajectories which does not accurately reflect the corresponding diagonal elements of the density matrix.

[19] It is worth noting that the classical motions along the nonadiabatic coupling vector both provide the coupling that causes the nonadiabatic transition and provide or accept the energy for the quantum transition to take place. Thus there is no formal difference between ''accepting'' modes and ''promoting'' modes in nonadiabatic dynamics.

[20] P. Pechukas, Phys. Rev. **181**, 174 (1969).

[21] E. J. Heller, J. Chem. Phys. **75**, 2923 (1981).

[22] See, for example, R. M. Stratt and M. Cho, J. Chem. Phys. **100**, 6700 (1994); M. Buchner, B. M. Ladanyi, and R. M. Stratt, *Ibid*. **97**, 8522 (1992), and references therein.

[23] E. R. Bittner and P. J. Rossky (manuscript in preparation).

[24] B. J. Schwartz and P. J. Rossky, J. Chem. Phys **101**, 6902 (1994); B. J. Schwartz and P. J. Rossky, *ibid*. **101**, 6917 (1994); D. Borgis and A. Staib, Chem. Phys. Lett. **230**, 405 (1994); B. J. Schwartz and P. J. Rossky, J. Mol. Liq. **65/66**, 23 (1995).

[25] B. J. Schwartz and P. J. Rossky, J. Phys. Chem. **98**, 4489 (1994); B. J. Schwartz and P. J. Rossky, Phys. Rev. Lett. **72**, 3282 (1994); B. J. Schwartz and P. J. Rossky, J. Phys. Chem. **99**, 2953 (1995).

[26] T. H. Murphrey and P. J. Rossky, J. Chem. Phys. **99**, 515 (1993).

[27] R. B. Barnett, U. Landmann and A. Nitzan, J. Chem. Phys. **90**, 4413 (1989).

[28] E. Keszei, S. Nagy, T. H. Murphrey and P. J. Rossky, J. Chem. Phys. **99**, 2004 (1993); E. Keszei, T. H. Murphrey and P. J. Rossky, J. Phys. Chem. **99**, 22 (1995).

[29] P. J. Rossky and J. Schnitker, J. Phys. Chem. **92**, 4277 (1988), and references therein.

[30] J. C. Alfano, P. K. Walhout, Y. Kimura, and P. F. Barbara, J. Chem. Phys. **98**, 5996 (1993); Y. Kimura, J. C. Alfano, P. K. Walhout, and P. F. Barbara, J. Phys. Chem. **98**, 3450 (1994); P. K. Walhout and P. F. Barbara (private communication).

[31] P. J. Reid, C. Silva, P. K. Walhout, and P. F. Barbara, Chem. Phys. Lett. **228**, 658 (1994).

[32] F. H. Long, H. Lu, and K. B. Eisenthal, Phys. Rev. Lett. **64**, 1469 (1990); F. H. Long, H. Lu, X. Shi, and K. B. Eisenthal, Chem. Phys. Lett. **185**, 47 (1991), and references therein.

[33] A. Migus, Y. Gauduel, J. L. Martin, and A. Antonetti, Phys. Rev. Lett. **58**, 1559 (1987); S. Pommeret, A. Antonetti, and Y. Gauduel, J. Am. Chem. Soc. **113**, 9105 (1991).

[34] F. H. Long, H. Lu, and K. B. Eisenthal, Chem. Phys. Lett. **160**, 464 (1989); Y. Gauduel, S. Pommeret, A. Migus, and A. Antonetti, J. Phys. Chem. **95**, 533 (1991).

[35] J. L. McGowen, H. M. Ajo, J. Z. Zhang, and B. J. Schwartz, Chem. Phys. Lett. **231**, 504 (1994).

[36] M. U. Sander, K. Luther, and J. Troe, Ber. Bunsen Ges. Phys. Chem. **97**, 953 (1993), and references therein.

[37] P. J. Rossky and J. D. Simon, Nature (London) **370**, 263 (1994).

[38] K. Toukan and A. Rahman, Phys. Rev. B **31**, 2643 (1985).

[39] J. Schnitker and P. J. Rossky, J. Chem. Phys. **86**, 3462 (1987).

[40] See, for example, M. P. Allen and D. J. Tildesley, *Computer Simulations of Liquids* (Oxford University, New York, 1987).

[41] O. V. Prezhdo and P. J. Rossky (manuscript in preparation).

[42] We deliberately avoid using the term ''in the first solvation shell'' since the excited state hydrated electron is an extended cylindrically symmetric object with a nodal plane in the center. In addition, the electron changes

size and shape as solvation proceeds, making it very difficult to rigorously define solvent shells for the electron. See Refs. 24, 41, and 44 for more details.

[43] The computed average excited state energy gap, at equilibrium, for the hydrated electron is 0.45 eV with a standard deviation of 0.15 eV (cf. Fig. 1).

[44] B. J. Schwartz and P. J. Rossky (in preparation).

[45] This finding of Neria and Nitzan played a role in our choice of identical coherence time for the electron in H_2O and D_2O; see Ref. 44.

[46] Real (quantum mechanical) water and heavy water have slightly different properties, however, primarily due to the difference in spatial dispersion between the proton and the deuteron. See, for example, G. S. Delbuono, P. J. Rossky, and J. Schnitker, J. Chem. Phys. **95**, 3728 (1991).

[47] A simple model assuming the nonadiabatic transition probability is inversely proportional to the quantum energy gap allows for an estimation of the transition rate from the equilibrium excited state (see Refs. 24 and 44). The rates were estimated from the population dynamics in the simulations to be 450 fs^{-1} for H_2O and 850 fs^{-1} for D_2O.

[48] Note that since the solvation dynamics take place on slightly different time scales in the two solvents, there would still be some minor differences in the observed transient spectroscopy. A spectral calculation based on the simulations which assumes identical nonadiabatic transition rates for H_2O and D_2O shows that at 300 fs time resolution, however, there would be little observable isotope effect. See Ref. 44.

[49] There are many issues in trying to determine the absolute magnitude of the nonadiabatic transition rate from simulations, the chief difficulty lying in the classical treatment of the solvent. For systems where the nonadiabatic coupling is linear in the spectral density of the bath, it is possible to make a ''quantum correction'' based on detailed balance and other factors to the semiclassically determined rate: see J. S. Bader and B. J. Berne, J. Chem. Phys. **100**, 8359 (1994), and references therein. These correction factors are not appropriate for the hydrated electron, however, as the nonadiabatic coupling is spread out throughout the solvent (Ref. 41) so that there is a distinctly nonlinear relationship between the coupling and the solvent spectral density.

[50] For example, the role of adiabaticity in biomolecular electron transfer reactions is explored in: A. Garg, J. N. Onuchic and V. Ambegaokar, J. Chem. Phys. **83**, 4491 (1985); J. N. Onuchic, *ibid*. **86**, 3925 (1987), and references therein.

[51] Electron transfer reactions can change from adiabatic to nonadiabatic in character with changes in the solvent parameters. See, for example, A. Masad, D. Huppert, and E. M. Kosower, Chem. Phys. **144**, 391 (1990).